

Strong-TransCenter: Improved Multi-Object Tracking based on Transformers with Dense Representations

Amit Galor* Roy Orfaig Ben-Zion Bobrovsky

School of Electrical Engineering, Tel-Aviv University

amitgalor@mail.tau.ac.il {royorfaig,bobrov}@tauex.tau.ac.il

Abstract

Transformer networks have been a focus of research in many fields in recent years, being able to surpass the state-of-the-art performance in different computer vision tasks. However, in the task of Multiple Object Tracking (MOT), leveraging the power of Transformers remains relatively unexplored. Among the pioneering efforts in this domain, TransCenter, a Transformer-based MOT architecture with dense object queries, demonstrated exceptional tracking capabilities while maintaining reasonable runtime. Nonetheless, one critical aspect in MOT, track displacement estimation, presents room for enhancement to further reduce association errors. In response to this challenge, our paper introduces a novel improvement to TransCenter. We propose a post-processing mechanism grounded in the Track-by-Detection paradigm, aiming to refine the track displacement estimation. Our approach involves the integration of a carefully designed Kalman filter, which incorporates Transformer outputs into measurement error estimation, and the use of an embedding network for target re-identification. This combined strategy yields substantial improvement in the accuracy and robustness of the tracking process. We validate our contributions through comprehensive experiments on the MOTChallenge datasets MOT17 and MOT20, where our proposed approach outperforms other Transformer-based trackers. The code is publicly available at: https://github.com/amitgalor18/STC_Tracker

1. Introduction

The task of multiple object tracking in video has been the center of much focus in computer vision research in the past few years, with various real-world applications (e.g. autonomous vehicles, sports analysis, surveillance, etc.). One of the most comprehensive benchmarks dedicated to this task is MOTChallenge [1], having several datasets such as MOT17 and MOT20 which consist of fully

annotated videos of pedestrians in various scenarios and environments. The goal of the tracker in the challenge is to infer the positions of each of the pedestrians in each frame while retaining their identities throughout the trajectories. There is a distinction in the challenge between online (causal) trackers which only use past and current frame information for the inference of a current frame and offline (non-causal) trackers that have access to information from all the video frames and can therefore infer on a current frame using future frame information. Much research was done using these datasets [2], with many trackers using different approaches to complete the task. One of the major breakthroughs in the field was SORT (Simple Online and Realtime Tracking) [3], having simplified the task and dividing it into several sub-tasks: Detection of all the pedestrians in the frame, association (Re-ID) between previous tracks (trajectories) and new detections, and prediction of track locations using a motion model. The association sub-task was done using the well-known Hungarian Algorithm [4], and the track prediction was done using a standard Kalman filter [5]. The method was further improved in the publication of DeepSORT [6], which introduced the use of a neural network for the detection subtask. Many more trackers in the following years used this Tracking-by-Detection paradigm [7]–[10], which introduced mainly improvement to the detector network and the track management methods, while some trackers featured a separate network for occlusion handling [11], advanced methods of assignment [12], [13] or camera motion compensation [7], [12], [14]. Other trackers proposed to combine the detection with other components (e.g., appearance embedding, motion model, association) in one module [8], [15]. In the last few years, several trackers [16]–[19] introduced frameworks based on Transformer networks [20] for MOT to benefit from the advantages of the generalizability of the model. The main advantage is the ability of the encoder-decoder architecture to encode features from the scene using a CNN (Convolutional Neural Network) [21] or PVT [22] while also encoding information about relationships between different parts of the scene and then decode the queries with a one-to-

*Corresponding author.

one assignment to objects. Transformer architectures have been shown to achieve better performance than CNN-based methods on several benchmarks, with great flexibility in the tasks they can complete [23]. Nevertheless, with limited data, transformer-based trackers still fall short of surpassing trackers based on state-of-the-art object detectors, either from detection imprecision or inaccurate track motion prediction.

The main contributions of this paper are summarized as follows: Our tracker is an attempt to improve upon a transformer-based tracker using post-processing methods for motion model estimation and re-identification. We show that a tuned Kalman filter performs better than the transformer motion tracking branch, and therefore reduces association errors. We introduce a modified implementation of the Kalman filter that is better optimized for the problem and includes integrated information from the network detection branch. As shown in 4.3 it indeed achieves better results in the HOTA and IDF1 evaluation metrics and competitive results on the MOTA metric on both MOT17 and MOT20 test datasets.

2. Related Work

Transformers. In Multiple Object Tracking, the input is a sequence of frames. The encoder-decoder transformer architecture is therefore designed to encode the representations of the frames, use self-attention to reason about the objects in the scene and the encoder-decoder attention to access information from the whole frame. The self attention helps preventing Identity Switches (IDSWs), terminate occluded tracks and initiate new tracks. Both Transtrack [17] and TrackFormer [16] use sparse object queries to detect new objects and initialize tracking based on the DETR (Detection Transformer) [23] architecture method, and track queries to keep information about the different objects across the frames, to achieve multi-frame attention. The most significant difference between the two is the association stage, in which TrackFormer took a point-based approach and TransTrack uses bounding-box-based association. MOTR [18] also employs a track query strategy but uses a temporal aggregation network to learn stronger temporal relations and obviate the need for IoU-based matching or Re-ID features. TransCenterV2 [19] took a different approach and achieved the best results out of all the Transformer-based trackers in the MOTChallenge benchmark [1], and therefore was chosen as the basis for our tracker. TransCenter trains pixel-wise dense queries to learn point-based tracking of pedestrian heatmap centers and sizes. They feed multi-scale tracking and detection queries into the decoder in order to find objects at different resolutions of the feature maps. It improved the efficiency by abandoning the heavy ResNet [21] based feature extraction and using the PVT (Pyramid Vision Transformer) [22]

architecture as an encoder. TransCenter also uses pixel-level dense queries for detection, to avoid the insufficient number and the overlapping nature of sparse queries without positional correlations. The track queries are kept active even when the object is not found for a few frames, in case it reappears after an occlusion. The main drawback is that the spatial information embedded into the query does not keep motion information from the past, limiting its accuracy and preventing the application for long term occlusions. **Kalman Filter.** Most of the trackers using the track-by-detection paradigm use the famous Kalman filter [5] to estimate the object’s motion model and hence predict the location of the object in each frame. Kalman filter is an efficient, unbiased, optimal minimum-error estimator for linear dynamics. The implementation of the Kalman filter that appeared in DeepSORT [6] was successfully used by many more modern trackers [8], [9], [24], [25], however this implementation can be improved with a careful choice of the state vector and measurement vector, as well as integration of additional information from the detector for the measurement noise estimation. Kalman filter allows a more precise association based on position, even in scenarios where the detector performs poorly, e.g., during occlusions or crowded scenes. **Re-ID.** Re-ID is the task of differentiating between different instances of the same class, and retaining the identity of an object seen in multiple occasions. Many works were conducted on optimal methods to represent an object’s appearance, either by multiple views or with a single camera [27]–[31], by using graph collaboration, clustering methods or dedicated neural networks. Retaining an object’s identity in a crowded scene is one of the main challenges in MOT. Several trackers use the same network for object detection and for extracting appearance features [8], [32] in order to increase efficiency, while other methods use a separate deep neural network to extract features from the detected objects [6], [25]. Several methods train both networks together in order to achieve both efficiency and high performance [24], [33]–[35]. A different approach utilized a GAN (Generative Adversarial Network) to augment the expected pose of the pedestrians in each frame [36]. The latest work [7] uses the Strong Baseline for person Re-identification [37] and the FastReID pytorch library [38], since this network achieves high performance on many person re-identification tasks. We chose this network since it was pre-trained on person re-identification datasets and has a simple implementation.

3. Proposed Method

3.1. Overview

Our tracker, STC (Strong-TransCenter) is based on TransCenter [19] with two main modifications integrated into the algorithm: A fine-tuned Kalman filter [5] and an Em-

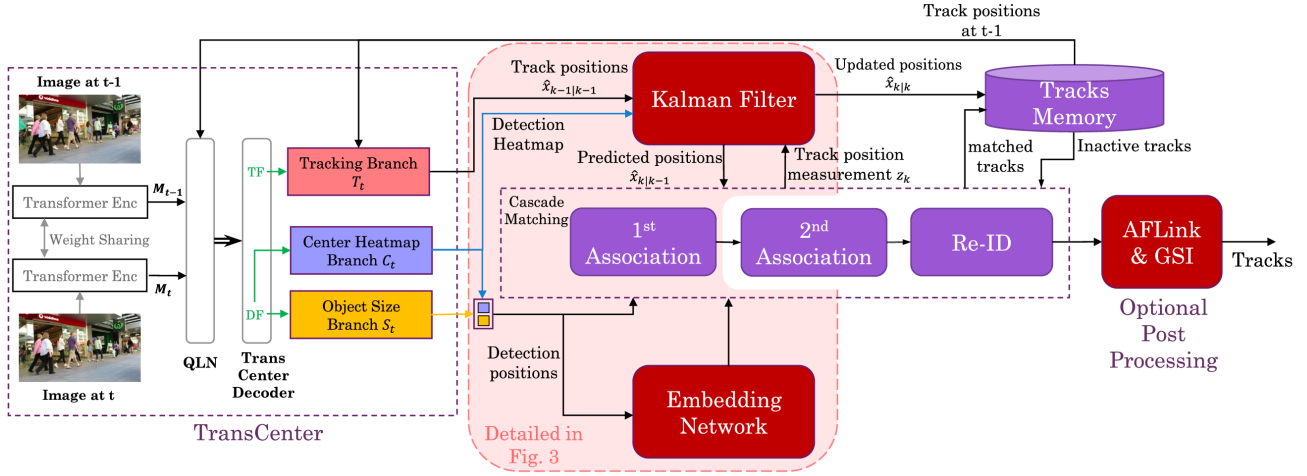


Figure 1: A flowchart overview of our STC tracker. The TransCenter [19] main architecture was simplified on the left. The additional blocks are in dark red (Kalman filter 3.2 and Embedding Network 3.3) and the modified blocks are in purple. The detection and track positions are used to calculate the GIoU distances [26], while the detection and track embeddings are used to calculate the appearance distance. The cascade matching contains two association steps that match new detections with existing tracks using a combined appearance and GIoU score. The Re-ID module attempts to match remaining detections with inactive tracks. The post-processing block is an optional addition, as in [7], [9], [25] and described in 4.4. The area in pink background is further detailed in Fig 3.

bedding Network based on FastReID [38]. A flowchart of our tracker pipeline is presented in Fig 1. The TransCenter main encoder-decoder architecture was kept as is. It takes as input two consecutive frames at a time and outputs the object location heatmaps with great performance. The modifications to the algorithm were focused on the track management, track localization and track-detection association. The cascade matching block contains two-step association depending on detection confidence as in [9], and a third Re-ID association. The first association stage matches active tracks in memory to new objects detected by the transformer with a high detection score. The second association stage matches the remaining active tracks with objects detected with low detection score. The third association matches the remaining detected objects with inactive tracks (tracks that were lost recently) and attempts to recover them back to the active tracks list. All three associations were adapted to include both a proximity score (GIoU - generalized Intersection over Union [26]) and an appearance score based on embedding from an Embedding network. An optional offline module was added and discussed in 4.4.

3.2. Kalman Filter

Kalman filter in a tracking task is used on trajectories to propagate each track’s location to the next frame (Kalman predict phase), while the Kalman motion model is updated every time a track is associated to a new detection (Kalman update phase). Given an estimated state vector:

$$\mathbf{x}_k = \phi_k \mathbf{x}_{k-1} + \mathbf{w}_k \quad (1)$$

Where ϕ_k is the state transition matrix and \mathbf{w}_k is a white processing noise, and an observation:

$$\mathbf{z}_k = \mathbf{H}_k \mathbf{x}_k + \mathbf{v}_k \quad (2)$$

Where \mathbf{z}_k is a measurement at frame k , \mathbf{H}_k is the observation matrix (the ideal relation between measurement and state vector), and \mathbf{v}_k is a white measurement noise, the two steps can be represented by these recursive equations for each frame $k \in \mathbb{N}$:

predict phase:

$$\begin{aligned} \hat{\mathbf{x}}_k^- &= \phi_k \hat{\mathbf{x}}_{k-1} \\ \mathbf{P}_k^- &= \phi_k \mathbf{P}_{k-1} \phi_k^\top + \mathbf{Q}_k \end{aligned} \quad (3)$$

update phase:

$$\begin{aligned} \mathbf{K}_k &= \mathbf{P}_k^- \mathbf{H}_k^\top (\mathbf{H}_k \mathbf{P}_k^- \mathbf{H}_k^\top + \mathbf{R}_k)^{-1} \\ \hat{\mathbf{x}}_k &= \hat{\mathbf{x}}_k^- + \mathbf{K}_k (\mathbf{z}_k - \mathbf{H}_k \hat{\mathbf{x}}_k^-) \\ \mathbf{P}_k &= (\mathbf{I} - \mathbf{K}_k \mathbf{H}_k) \mathbf{P}_k^- \end{aligned} \quad (4)$$

Where $\hat{\mathbf{x}}_k^-$ is the prior estimate, $\hat{\mathbf{x}}_k$ is the updated estimate, \mathbf{P}_k is the updated estimate covariance matrix, \mathbf{P}_k^- is the prior estimate covariance matrix \mathbf{K}_k is the Kalman gain, \mathbf{Q}_k is the process noise covariance, and \mathbf{R}_k is the measurement noise covariance. The implementation we chose was based on the work of DeepSORT [6] but the state vector and measurement representation were amended:

$$\mathbf{x} = [x_c, y_c, w, h, \dot{x}_c, \dot{y}_c, \dot{w}, \dot{h}]^\top \quad (5)$$

Where (x_c, y_c) are the 2D coordinates of the object center in the image plane. w is the bounding box width and h is the bounding box height. We replaced the aspect ratio in the state vector with the object width, to avoid non-linearity caused by division by small numbers. Many works [6], [9], [24], [25] used an implementation that converts the measurement vector from the detector network, usually taking the form:

$$\zeta = [x_{tl}, y_{tl}, x_{br}, y_{br}] \quad (6)$$

to the same form of the state vector:

$$\mathbf{z} = [x_c, y_c, a, h] \quad (7)$$

Where (x_{tl}, y_{tl}) are the top left corner coordinates and (x_{br}, y_{br}) are the bottom right corner coordinates. Accordingly, the common implementations choose the observation matrix to be the trivial projection matrix from state space to measurement space for the 4 position arguments, and zeros for the 4 velocity arguments:

$$\tilde{\mathbf{H}} = [\mathbf{I}]_{4 \times 4} [\mathbf{0}]_{4 \times 4} \quad (8)$$

However, as seen in equation 2, the measurement noise \mathbf{v}_k is not included in this conversion. In order to get a more accurate estimation of the noise, we chose to use the original measurement such that $z = \zeta$ and the transformation will be done using the observation matrix:

$$\mathbf{H} = \begin{bmatrix} 1 & 0 & -\frac{1}{2} & 0 & 0 & 0 & 0 & 0 \\ 0 & 1 & 0 & -\frac{1}{2} & 0 & 0 & 0 & 0 \\ 1 & 0 & \frac{1}{2} & 0 & 0 & 0 & 0 & 0 \\ 0 & 1 & 0 & \frac{1}{2} & 0 & 0 & 0 & 0 \end{bmatrix} \quad (9)$$

Moreover, in order to get a more accurate estimate of the measurement error of the detector, we used the detection heatmap that is predicted by the transformer network before the creation of the detection bounding boxes. For each detection peak in the heatmap, we calculated the FWHM (Full Width Half Maximum) around the peak in the x and y directions, as demonstrated in Fig 2. The heatmap can be correlated to a probability distribution, and it is known that for a Gaussian distribution with standard deviation σ :

$$\text{FWHM} \propto \sigma \quad (10)$$

Therefore we modified \mathbf{R} , the covariance matrix of measurement noise \mathbf{v}_k , introduced in equation 2, as follows:

$$\mathbf{R} = \begin{bmatrix} \alpha \cdot F_x^2 & 0 & 0 & 0 \\ 0 & \alpha \cdot F_y^2 & 0 & 0 \\ 0 & 0 & \alpha \cdot F_x^2 & 0 \\ 0 & 0 & 0 & \alpha \cdot F_y^2 \end{bmatrix} \quad (11)$$

Where F_x and F_y are the FWHM of the relevant detection in directions x and y respectively, and $\alpha = 1$ is a constant, chosen after optimization. Different combinations of

FWHM, constants, and the original width and height measures were tested and the best results were achieved with the simple approach presented in equation 11. We found that this modification is particularly helpful in scenes with a dynamic camera or objects with varying sizes such as those in the MOT17 dataset, and not very helpful in scenes with a static camera and objects of roughly the same size, such as those in the MOT20 dataset. The integration of motion

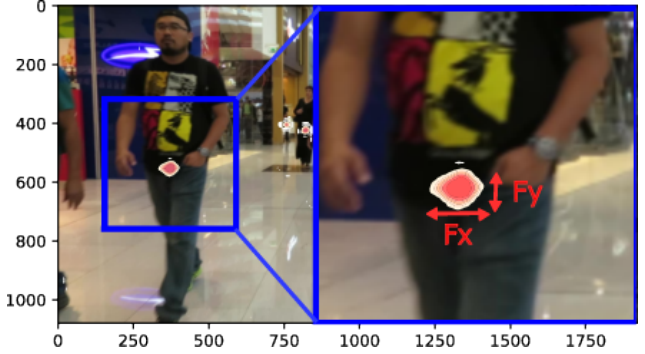


Figure 2: Visualization of the FWHM calculation. The TransCenter Transformer predicts a heatmap of the object detections. The blue window on the right is a zoom-in on an area in the left of the frame. The width of each peak (FWHM) is calculated in the x and y direction, and is denoted by F_x and F_y .

model estimation allows a more precise track position estimation and prevents misdetections and IDSWs, especially in cases where the detection is difficult.

3.3. Embedding Network

In order to tackle the problem of IDSWs, especially in cases of crowded scenes with many possible matches in close proximity, we incorporated a method to base association on appearance instead of only GIoU. The implementation we chose was the FastReID library [38], based on the SBS architecture [37] with ResNeSt50 backbone [39]. The model was trained on the MOT17 and MOT20 train sets as in [7]. Attempts were made to use the features derived from the TransCenter transformer itself as the object embeddings but it achieved poor results compared to the SBS network, which was trained specifically for the Re-ID task. The network creates an embedding vector to represent the image patch containing the detected object using the heatmap centers' locations from the transformer. After every matching with a high enough detection score, the embedding vector is updated as the new appearance of the associated track. This is because a low score detection from the transformer network usually correlates with a problematic visual detection, e.g., a partially occluded object, that does not represent the object's regular appearance. The update is applied using an EMA (Exponential Moving Average), as in [7] and [8]. The

embedding vector for track i at frame k will be therefore updated as such:

$$e_i^k = \alpha e_i^{k-1} + (1 - \alpha) f_i^k \quad (12)$$

Where f_i^k is the appearance embedding of the current matched detection and $\alpha = 0.9$ is a momentum term.

As demonstrated in Fig 3, the difference between our suggested association and the association of the baseline Transcenter is both the integrated Kalman filter and the added Embedding network that allows a combined distance for matching. In every association stage an embedding distance is calculated between all the existing tracks and the new detections, as the cosine similarity between the track embedding e_i^k and the new detection embedding vector f_j^k . As in [7], the combination of GIoU score and appearance embedding score was done by taking the minimum value between the two:

$$C_{i,j} = \min\{d_{i,j}^{giou}, \hat{d}_{i,j}^{emb}\} \quad (13)$$

Where $C_{i,j}$ is the (i,j) element of cost matrix C . $d_{i,j}^{giou}$ is the GIoU distance between the i -th track bounding box and the j -th detection bounding box, representing the motion cost. $d_{i,j}^{emb}$ is the cosine distance between the average track appearance vector i and the new detection appearance embedding j . $\hat{d}_{i,j}^{emb}$ is our new appearance cost. Before combining the distances we filter out potential matches that don't comply with chosen thresholds for appearance distance and GIoU distance. The chosen set of thresholds differs in our case since we used GIoU [26]) instead of the regular IoU. The thresholds were chosen empirically using a grid search. The association itself, after creating the cost matrix, is done using the Hungarian algorithm [4].

4. Experiments

4.1. Dataset and Evaluation Metrics

The experiments were conducted on the MOT17 dataset [1] which is composed of 7 videos for training and 7 videos for testing, and the MOT20 dataset [40] which is composed of 4 videos for training and 4 videos for testing. The videos feature many pedestrians in various natural scenarios (streets, shopping centers etc.) with different lighting conditions, static or moving camera, different camera fps and resolution etc. The train set contains annotation files with bounding box locations for every object in every frame. The test set has only the videos available while performance evaluation is done using the MOTchallenge website with restrictive measures to avoid overfitting. Methods in the MOTChallenge are evaluated using several main metrics.

MOTA (Multiple Object Tracking Accuracy) [41] has been used as the main evaluation metric for MOT for many

years. It is calculated by the formula:

$$MOTA = 1 - \frac{FN + FP + IDSW}{GT} \quad (14)$$

Where FN , FP , $IDSW$, and GT are the numbers of false negatives (misses), false positives, IDSWs and ground truth labels respectively in all the frames of the sequence. This metric places a greater emphasis on detection-based errors and is therefore more useful when evaluating a tracker's detector.

MOTP (Multiple Object Tracking Precision) [41] is the measure of position precision, regardless of the detection and identification skills of the tracker. It is calculated as:

$$MOTP = \frac{D}{M} \quad (15)$$

Where D is the sum of distances between predicted positions and ground truth positions, and M is the number of matches found for all frames.

IDF1 [42] is a measurement of the tracker's ability to retain all of the objects' identifications throughout the sequence, and is based on the standard F1 score that balances between precision and recall in classification tasks. It is widely used in the MOTChallenge benchmark and is calculated by the formula:

$$IDF1 = \frac{2IDTP}{2IDTP + IDFP + IDFN} \quad (16)$$

Where $IDFP$, $IDFN$ and $IDTP$ are identification false positive matches, false negative matches and true positive matches.

HOTA (Higher Order Tracking Accuracy) [43] is a relatively new evaluation metric that aims to balance between the ability of a tracker to detect all objects and associate their individual identifications in one number. It is calculated by the formula:

$$HOTA = \sqrt{\frac{\sum_c \mathcal{A}(c)}{|TP| + |FN| + |FP|}} \quad (17)$$

$$\mathcal{A}(c) = \frac{|TPA(c)|}{|TPA(c)| + |FNA(c)| + |FPA(c)|}$$

Where TP , FN , and FP are the detection true positives, false negatives, and false positives respectively, and each TP of interest c has a weighted metric $\mathcal{A}(c)$ that weighs the association true positives, false negatives and false positives TPA , FNA and FPA , as thoroughly explained and illustrated in [43]. This evaluation method produces more intuitive performance scores in many scenarios, so we consider it a better evaluation metric for the MOT task.

MT (Mostly Tracked) and **ML** (Mostly Lost) metrics are intended to get an intuitive sense of the extreme cases of the

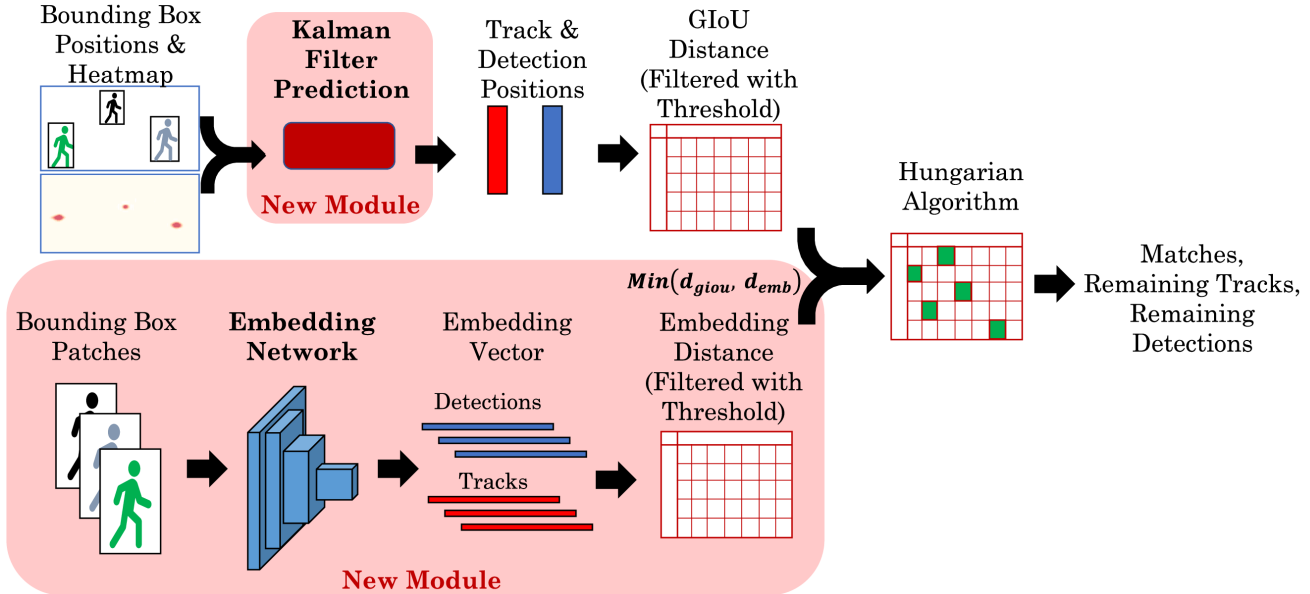


Figure 3: The main contributions of this paper: A flowchart of the modified association stage. The new modules are in the red background, and correspond to the Kalman, Embedding and 1st Association blocks from Fig 1. The fine-tuned Kalman filter uses information from the detection heatmap to improve the GIoU distance accuracy, while the appearance embedding distance helps in cases of pedestrians crowded together. The Hungarian algorithm for linear association is then applied to the resulting cost matrix. The process is then repeated for the 2nd Association and Re-ID stages, as seen in Fig 1.

best and worst trajectories to complement the MOTA metric which averages everything, but they are ambivalent to IDSWs. Therefore, like MOTA, these metrics give greater emphasis to the detector performance.

4.2. Implementation

Our proposed method was implemented in Python and is available on GitHub. The inference run for our submitted MOTChallenge results was done on a computer with an Intel Xeon Silver 4110 CPU, and a Geforce GTX 1180 Graphics card with 8GB VRAM. We conducted the execution of the original TransCenter method on the same hardware configuration to recreate their results and directly compare it to our proposed method. This comparison encompassed performance metrics as well as runtime. Notably, our STC tracker demonstrated only a slight decrease in FPS (7%-17%) compared to the TransCenter baseline, primarily attributed to the additional embedding network. Running our tracker without the embedding network yielded the exact same FPS as the baseline, highlighting that our performance improvements did not significantly impact runtime efficiency. Please note that we did not include an FPS (runtime) column in our results table due to variations in hardware configurations across different methods in the literature. While we executed our proposed STC tracker and the original TransCenter method on the same hardware for a direct performance comparison, many published methods em-

ployed significantly more powerful hardware setups. Therefore, adding FPS values to the table could lead to misleading comparisons. The results rely on a series of thresholds for different parts of the pipeline. The high detection threshold for the first association stage is 0.3 in MOT17 and 0.5 in MOT20, and the low detection threshold for the second association stage is 0.1, based on the detection confidence score as in [19]. The threshold for the embedding distance and GIoU distance are 0.4 and 1.0 respectively. Based on the combined distance, the matching threshold for the linear association itself is 0.9 for the first association and the Re-ID recovery association, and 0.4 for the second association, since the second association considers detections with lower confidence.

4.3. Results

Table I and Table II present results on the MOT17 and MOT20 test datasets, respectively. We can see that STC outperforms the trackers that used the same pretraining conditions in terms of the HOTA and IDF1 metrics by a great margin, while the MOTA metric, MT and ML are roughly the same as the baseline tracker. Our MOTP is similar to TransCenter as expected, since the track positions after the association stage are taken as the detection positions. The FN and FP measures can be quite noisy since they are very sensitive to tracking thresholds, thus they are not reliable evaluators by themselves, but the balance between them can

indicate different tendencies of trackers to prefer misdetection over false-detection or vice versa. The combination of the lower IDSW rate and the similar FN rate compared to the baseline tracker demonstrates both the performance of the accurate detection process by the original TransCenter transformer [19], and the ability of the Kalman filter and improved association to track more consistently. It is worth noting that STC outperforms all of the transformer-based methods in the HOTA and IDF1 metrics.

4.4. Offline modules

The tracker we presented is an **online** tracker (causal), which means it generates the prediction for the track locations on each frame only based on information from the current and previous frames. Other trackers [25], [53], [54] developed methods for offline tracking (non-causal), which have the advantage of using information from future frames as well. These trackers can be used for various tasks such as sports analysis or analysis of past surveillance videos, but not for real-time tasks which require immediate response. Nevertheless, we decided to test two non-causal features in our ablation study 4.5 - AFLink and GSI, both of which were developed in the work of StrongSORT [25].

AFLink (Appearance-Free Link) is a linking algorithm, predicting connectivity between two trajectories based on the spatio-temporal information, i.e., the change of their respective positions through time. It is essentially able to conclude whether two predicted tracks by the original tracker are in fact from the same object and therefore decrease the number of IDSWs.

GSI (Gaussian-smoothed Interpolation) is an interpolation algorithm, intended to fill gaps in predicted trajectories by the original tracker. It models the trajectory as a gaussian process with a function kernel in order to interpolate the track’s position in the missing segment.

4.5. Ablation Study

In our ablation study we compared the added modules described in 3 that make up our proposed method STC, as well as the offline modules described in 4.4 that we explored on top of STC and the original TransCenter [19]. The AFLink and GSI modules are the non-causal features developed in [25] and described in 4.4. As we can see in the results Table III the AFLink module mainly improves the IDSW number and has no significant effect on the main metrics. The GSI module has a significant effect on the number of FP (false positives) and FN (false negatives, i.e., misdetections) since it was able to complete missing trajectories but at the same time generated false trajectories, and the balance between them indeed improved the main evaluation metrics in several configurations, depending on parameters of the GSI function. In order to optimize the association step between tracks and new detections we tested

association using only the appearance embeddings (noted as "Only Embedding"), with the addition of the default implementation of the Kalman filter based on DeepSORT [6] (noted as "Default Kalman") and with the addition of our improved implementation of the Kalman filter (noted as "Improved Kalman"). The improved Kalman and the embedding network together make up our STC tracker. Using only the embedding distance caused a very high number of IDSW and poor metric results as expected, since it caused the association to match tracks and detections with no regard to their positions. Using only the improved Kalman filter, without using the embedding distance, i.e., not using the appearance feature at all, caused a slightly smaller number of FP but higher number of IDSW. We can also see that the improved Kalman filter contributes to all the metrics compared to the default Kalman implementation, which confirms that modifying the state vector, correcting the measurement projection matrix and adapting the measurement noise covariance matrix using the detection heatmap FWHM are an effective way to fine-tune the tracker to the required task. The last experiment is testing the classic method of fusing the embedding and GIoU scores for the final association distance, using the formula:

$$Dist = \lambda \cdot d_{emb} + (1 - \lambda) \cdot d_{giou} \quad (18)$$

Where $Dist$ is the fused association distance, d_{emb} is the appearance embedding distance, d_{giou} is the bounding box GIoU distance and λ is a configurable parameter for the respective weight, that we chose as 0.5 for this example after testing various values. We found that like in [7] the best way to utilize the information from the embedding distances is by using the minimum between the two distances. The minimum is taken after filtering the GIoU distance with a higher threshold to guarantee the track predicted position and the positions of the potential matches are close, before considering a match based on appearance.

4.6. Qualitative Analysis

Another method of analysis included plotting bounding boxes to indicate true positive tracking (TP) in green, false negative (FN) in red and false positive (FP) in pink. An additional example for improved tracking is demonstrated in Fig 6, in which the indicated boxes show a pedestrian that is almost entirely occluded and was detected by the Transformer attention mechanism in the wrong position, but the addition of a motion model made it possible to associate it to the existing track in our STC tracker. The original TransCenter managed to detect the mostly occluded pedestrian but positioned the track in the wrong location, causing both an FN in the ground truth location and an FP in the tracker predicted location. Our STC tracker managed to predict the correct location in this scenario due to the added Kalman-based motion model. This demonstrates both the ability of

Table 1: Results on MOT17 test set on public and private detections. The methods chosen for comparison use the same dataset for pretraining or additional datasets, indicated by the background color. The best result among methods trained in the same conditions is in **bold**.

Method	Public Detections										Private Detections										
	Data	MOTA ↑	MOTP ↑	IDF1 ↑	HOTA ↑	MT ↑	ML ↓	FP ↓	FN ↓	IDSW ↓	Data	MOTA ↑	MOTP ↑	IDF1 ↑	HOTA ↑	MT ↑	ML ↓	FP ↓	FN ↓	IDSW ↓	
GSDT [44]											5d1	66.2	79.9	68.7	55.5	40.8	18.3	43,368	144,261	3,318	
SOTMOT [32]	5d1	62.8		67.4		24.4	33.0	6,556	201,319	2,017	5d1	71.0		71.9		42.7	15.3	39,537	118,983	5,184	
GSDT_V2 [44]											5d1	73.2		66.5	55.2	41.7	17.5	26,397	120,666	3,891	
CorrTracker [35]											5d1	76.5		73.6	60.7	47.6	12.7	29,808	99,510	3,369	
FairMOT [24]											5d1+CH	73.7	81.3	72.3	59.3	43.2	17.3	27,507	117,477	3,303	
RelationTrack [33]											5d1+CH	73.8	81.0	74.7	61.0	41.7	23.2	27,999	118,623	1,374	
CSTrack [34]											5d1+CH	74.9	80.9	72.6	59.3	41.5	17.5	23,847	114,303	3,567	
MLT [45]											(5d1+CH)	75.3	81.7	75.5		49.3	19.5	27,879	109,836	1,719	
FUFET [46]											(5d1+CH)	76.2	81.1	68.0	57.9	51.1	13.6	32,796	98,475	3,237	
TransCenterV2 [19]	5d1+CH	76.0	81.4	65.6		47.3	15.3	28,369	101,988	4,972	5d1+CH	76.4	81.2	65.4		51.7	11.6	37,005	89,712	6,402	
MOTDT17 [47]	RE1	50.9	76.6	52.7	41.2	17.5	35.7	24,069	250,768	2,474											
UnsupTrack [13]	PT	61.7	78.3	58.1	46.9	27.2	32.4	16,872	197,632	1,864											
GMT_CT [48]	RE2	61.5		66.9		26.3	32.1	14,059	200,655	2,415											
TrackFormer [16]	CH	62.5		60.7		29.8	26.9	14,966	206,619	1,189	CH	74.1			68.0	57.3	47.3	10.4	34,602	108,777	2,829
SiamMOT [49]	CH	65.9		63.5		34.6	23.9	18,098	170,955	3,040											
MOTR [18]	CH	67.4		67.0		34.6	24.5	32,355	149,400	1,992											
CenterTrack [50]											CH	73.4			68.6	57.8					2,439
TraDeS [51]											CH	67.8	78.4	64.7		34.6	24.6	18,489	160,332	3,039	
PermaTrack [52]											CH	69.1		63.9	52.7	36.4	21.5	20,892	150,060	3,555	
TransTrack [17]											CH	73.8		68.9	55.5	43.8	17.2	28,998	114,104	3,699	
TransCenterV2 [19]	CH	75.9	81.2	65.9	56.7	49.8	12.1	30,190	100,999	4,626	CH	75.2		63.5	54.1	55.3	10.2	50,157	86,442	3,603	
STC (ours)	CH	75.9	81.2	72.8	60.2	50.2	11.6	34,615	98,617	2,860	CH	75.9	81.0	72.7	60.3	54.3	7.3	45,939	86,748	3,177	

Table 2: Results on MOT20 testset on public and private detections. The methods chosen for comparison use the same dataset for pretraining or additional datasets, indicated by the background color. The best result within the same training conditions (background color) is in **bold**.

Method	Public Detections										Private Detections									
	Data	MOTA ↑	MOTP ↑	IDF1 ↑	HOTA ↑	MT ↑	ML ↓	FP ↓	FN ↓	IDSW ↓	Data	MOTA ↑	MOTP ↑	IDF1 ↑	HOTA ↑	MT ↑	ML ↓	FP ↓	FN ↓	IDSW ↓
CorrTracker [35]											5d1	65.2		69.1		66.4	8.9	79,429	95,855	5,183
GSDT_V2 [44]											5d1	67.1		67.5	53.6	53.1	13.2	31,507	135,395	3,230
GSDT [44]											5d1	67.1	79.1	67.5	53.6	53.1	13.2	31,913	135,409	3,131
SOTMOT [32]											5d1	68.6		71.4	57.4	64.9	9.7	57,064	101,154	4,209
FairMOT [24]											5d1+CH	61.8	78.6	67.3	54.6	68.8	7.6	103,440	88,901	5,243
CSTrack [34]											5d1+CH	66.6	78.8	68.6	54.0	50.4	15.5	25,404	144,358	3,196
RelationTrack [33]											5d1+CH	67.2	79.2	70.5	56.5	62.2	8.9	61,134	104,597	4,243
TransCenterV2 [19]	5d1+CH	72.4	81.2	57.9		64.2	12.3	25,121	115,421	2,290	5d1+CH	72.5	81.1	58.1		64.7	12.2	25,722	114,310	2,332
UnsupTrack [13]	PT	53.6	80.1	50.6	41.7	30.3	25.0	6,439	231,298	2,178	CH	65.0		50.1	48.9		13.4	27,191	150,197	3,608
TransTrack [17]											CH	68.6		65.7	54.7	53.6	14.6	20,348	140,373	1,532
TrackFormer [16]											CH	72.9	81.0	57.7	50.2	66.5	11.8	28,596	108,982	2,625
TransCenterV2 [19]	CH	72.8	81.0	57.6	50.1	65.5	12.1	28,026	110,312	2,621	CH	72.9	81.0	68.2	56.4	66.8	11.9	28,892	109,309	1,791
STC (Ours)	CH	72.8	81.0	68.1	56.4	65.9	12.1	28,167	110,687	1,769	CH	72.9	81.0	68.2	56.4	66.8	11.9	28,892	109,309	1,791

the transformer attention mechanism to infer the existence of occluded objects and the assistance of the motion model in predicting the location of lost objects.

5. Conclusion

In this paper, we explored the problem of multi-object tracking and demonstrated the potential of a Transformer-based tracker on the MOTChallenge MOT17 and MOT20 benchmark datasets. We addressed one of the weakest components of the transformer - its motion estimation branch - and demonstrated the benefits of including a fine-tuned Kalman filter for motion estimation while choosing a more accurate representation of the measurement vector and estimating its error. Moreover, we found that integrating a combination of appearance embedding and position in the track association stage reduces association errors as demonstrated by the IDF1 metric. Our tracker is currently ranked first among the transformer-based trackers in the MOTChal-

lenge datasets in terms of HOTA and IDF1, indicating the merits of our modifications. Looking ahead, we believe future research into transformers and their tailored implementation for the MOT task might lead to an all-in-one transformer based tracker without the need for additional modules.

Acknowledgement

We thank Shlomo Shmeltzer Institute for Smart Transportation at Tel-Aviv University for the scholarship for the first author and for the support of our Autonomous Mobile Laboratory.

References

- [1] A. Milan, L. Leal-Taixe, I. Reid, S. Roth, and K. Schindler, "Mot16: A benchmark for multi-object tracking," *arXiv*, Mar. 2016.

Table 3: Ablation study of different components of our tracker. The experiments were conducted on the mot17 train dataset using private detections. The rows in **dark blue** text are offline options. Best results are underlined, best online results are in **bold**.

Setting	MOTA \uparrow	IDF1 \uparrow	HOTA \uparrow	FP \downarrow	FN \downarrow	IDSW \downarrow
TransCenterV2	86.9	77.3	70.4	1272	12813	678
TransCenterV2 + AFLink	86.9	79.9	71.7	<u>1251</u>	12892	603
TransCenterV2 + GSI	87.0	77.2	70.4	2442	11490	663
TransCenterV2 + AFLink + GSI	87.1	79.9	71.9	2306	11583	565
TransCenterV2 + Default Kalman	86.7	82.0	73.0	1553	12779	622
TransCenterV2 + Improved Kalman	86.8	82.7	73.4	1539	12783	524
TransCenterV2 + Default Kalman + Embedding	86.7	82.8	73.6	1611	12802	583
STC	86.8	83.6	73.9	1581	12750	453
STC + AFLink	86.8	83.1	73.6	1563	12798	436
STC + GSI	<u>88.3</u>	<u>84.0</u>	<u>74.6</u>	2057	<u>10782</u>	329
STC + AFLink + GSI	88.2	83.6	74.4	2145	10784	<u>305</u>
STC Only Embedding	85.7	76.2	69.5	1435	12767	1820
STC Fused Embedding & GIoU	86.7	80.5	72.3	1325	12789	624

- [2] W. Luo, J. Xing, A. Milan, X. Zhang, W. Liu, and T.-K. Kim, "Multiple object tracking: A literature review," *Artificial Intelligence*, vol. 293, p. 103448, Apr. 2021, ISSN: 00043702. DOI: [10.1016/j.artint.2020.103448](https://doi.org/10.1016/j.artint.2020.103448).
- [3] A. Bewley, Z. Ge, L. Ott, F. Ramos, and B. Uppcroft, "Simple online and realtime tracking," in *2016 IEEE International Conference on Image Processing (ICIP)*, L. Karam, Ed., Feb. 2016, pp. 3464–3468. DOI: [10.1109/ICIP.2016.7533003](https://doi.org/10.1109/ICIP.2016.7533003).
- [4] H. W. Kuhn, "The hungarian method for the assignment problem," *Naval Research Logistics Quarterly*, vol. 2, pp. 83–97, 1-2 Mar. 1955, ISSN: 00281441. DOI: [10.1002/nav.3800020109](https://doi.org/10.1002/nav.3800020109).
- [5] R. G. Brown and P. Y. Hwang, *Introduction to random signals and applied Kalman Filtering*, 4th. Wiley, 2012, ISBN: 978-0-470-60969-9.
- [6] N. Wojke, A. Bewley, and D. Paulus, "Simple online and realtime tracking with a deep association metric," in *2017 IEEE International Conference on Image Processing (ICIP)*, X. Lin, Ed., IEEE, Sep. 2017, pp. 3645–3649, ISBN: 978-1-5090-2175-8. DOI: [10.1109/ICIP.2017.8296962](https://doi.org/10.1109/ICIP.2017.8296962).
- [7] N. Aharon, R. Orfaig, and B.-Z. Bobrovsky, "Bot-sort: Robust associations multi-pedestrian tracking," *arXiv*, Jun. 2022.
- [8] Z. Wang, L. Zheng, Y. Liu, Y. Li, and S. Wang, "Towards real-time multi-object tracking," in *Computer Vision – ECCV 2020*, A. Vedaldi, H. Bischof, T. Brox, and J.-M. Frahm, Eds., Cham: Springer International Publishing, 2020, pp. 107–122, ISBN: 978-3-030-58621-8.
- [9] Y. Zhang, P. Sun, Y. Jiang, *et al.*, "Bytetrack: Multi-object tracking by associating every detection box," in *Computer Vision – ECCV 2022*, S. Avidan, G. Brostow, M. Cissé, G. M. Farinella, and T. Hassner, Eds., Cham: Springer Nature Switzerland, 2022, pp. 1–21, ISBN: 978-3-031-20047-2.
- [10] D. Stadler and J. Beyerer, "Improving multiple pedestrian tracking by track management and occlusion handling," in *2021 IEEE/CVF Conference on Computer Vision and Pattern Recognition (CVPR)*, D. Forsyth, G. Gkioxari, T. Tuytelaars, R. Yang, and J. Yu, Eds., IEEE, Jun. 2021, pp. 10953–10962, ISBN: 978-1-6654-4509-2. DOI: [10.1109/CVPR46437.2021.01081](https://doi.org/10.1109/CVPR46437.2021.01081).
- [11] T. Liu, W. Luo, L. Ma, J.-J. Huang, T. Stathaki, and T. Dai, "Coupled network for robust pedestrian detection with gated multi-layer feature extraction and deformable occlusion handling," *IEEE Transactions on Image Processing*, vol. 30, pp. 754–766, 2021, ISSN: 1057-7149. DOI: [10.1109/TIP.2020.3038371](https://doi.org/10.1109/TIP.2020.3038371).
- [12] D. Stadler and J. Beyerer, "Modelling ambiguous assignments for multi-person tracking in crowds," in *2022 IEEE/CVF Winter Conference on Applications of Computer Vision Workshops (WACVW)*, R. Farrell, C. Zhao, S. Anand, and R. Souvenir, Eds., IEEE, Jan.

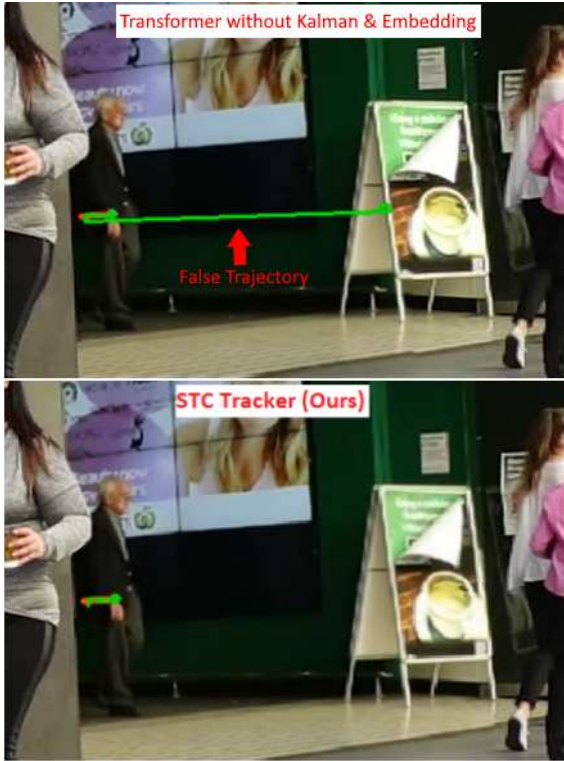


Figure 4: Visualization of a specific scenario in the results of a tracker based only on transformer (TransCenterV2 [19]) at the top and our STC tracker results (Transformer with Kalman and Embedding) at the bottom. The green trajectories are the tracker prediction with a history of 20 frames and the orange trajectories are the ground truth positions. An IDSW has occurred in the top image, and is demonstrated by the big "jump" in the trajectory from right to left, giving the new pedestrian that emerged an existing track ID. In the bottom image the trajectory only began when the pedestrian emerged. The results are from the MOT17-09 video on frame 389.

2022, pp. 133–142, ISBN: 978-1-6654-5824-5. DOI: [10.1109/WACVW54805.2022.00019](https://doi.org/10.1109/WACVW54805.2022.00019).

- [13] S. Karthik, A. Prabhu, and V. Gandhi, "Simple unsupervised multi-object tracking," *arXiv*, Jun. 2020.
- [14] P. Bergmann, T. Meinhardt, and L. Leal-Taixe, "Tracking without bells and whistles," I. S. Kweon, N. Paragios, M.-H. Yang, and S. Lazebnik, Eds., IEEE, Oct. 2019, pp. 941–951, ISBN: 978-1-7281-4803-8. DOI: [10.1109/ICCV.2019.00103](https://doi.org/10.1109/ICCV.2019.00103).
- [15] A. Milan, S. H. Rezatofghi, A. Dick, I. Reid, and K. Schindler, "Online multi-target tracking using recurrent neural networks," *Proceedings of the AAAI Conference on Artificial Intelligence*, vol. 31, 1 Feb.

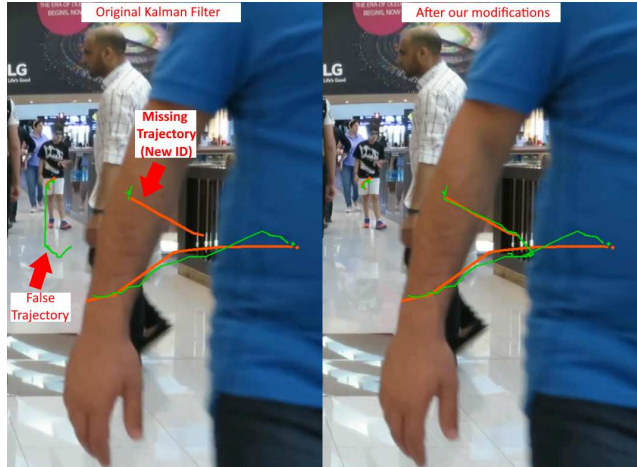


Figure 5: Visualization of a specific scenario in the results of our tracker when based on the default Kalman implementation seen in many works [6], [9], [24], [25], compared with our tracker after the modifications to the Kalman filter. The green trajectories are the tracker prediction with a history of 20 frames and the orange trajectories are the ground truth positions. The image on the left shows a person reappearing from the right after an occlusion and receiving a new ID by the tracker, while a new person in the back appears in the frame and receives a false existing ID with a long history. In the image on the right, both errors are corrected with the modified Kalman filter. The results are from the MOT17-11 video on frame 720.

2017, ISSN: 2374-3468. DOI: [10.1609/aaai.v31i1.11194](https://doi.org/10.1609/aaai.v31i1.11194).

- [16] T. Meinhardt, A. Kirillov, L. Leal-Taixe, and C. Feichtenhofer, "Trackformer: Multi-object tracking with transformers," *arXiv*, Jan. 2021.
- [17] P. Sun, J. Cao, Y. Jiang, *et al.*, "Transtrack: Multiple object tracking with transformer," *arXiv*, Dec. 2020.
- [18] F. Zeng, B. Dong, Y. Zhang, T. Wang, X. Zhang, and Y. Wei, "Motr: End-to-end multiple-object tracking with transformer," in *Computer Vision – ECCV 2022*, S. Avidan, G. Brostow, M. Cissé, G. M. Farinella, and T. Hassner, Eds., Cham: Springer Nature Switzerland, 2022, pp. 659–675, ISBN: 978-3-031-19812-0.
- [19] Y. Xu, Y. Ban, G. Delorme, C. Gan, D. Rus, and X. Alameda-Pineda, "Transcenter: Transformers with dense representations for multiple-object tracking," *IEEE Transactions on Pattern Analysis and Machine Intelligence*, pp. 1–16, 2022. DOI: [10.1109/TPAMI.2022.3225078](https://doi.org/10.1109/TPAMI.2022.3225078).
- [20] A. Vaswani, N. Shazeer, N. Parmar, *et al.*, "Attention is all you need," *NeurIPS*, pp. 5998–6008, Jun. 2017.

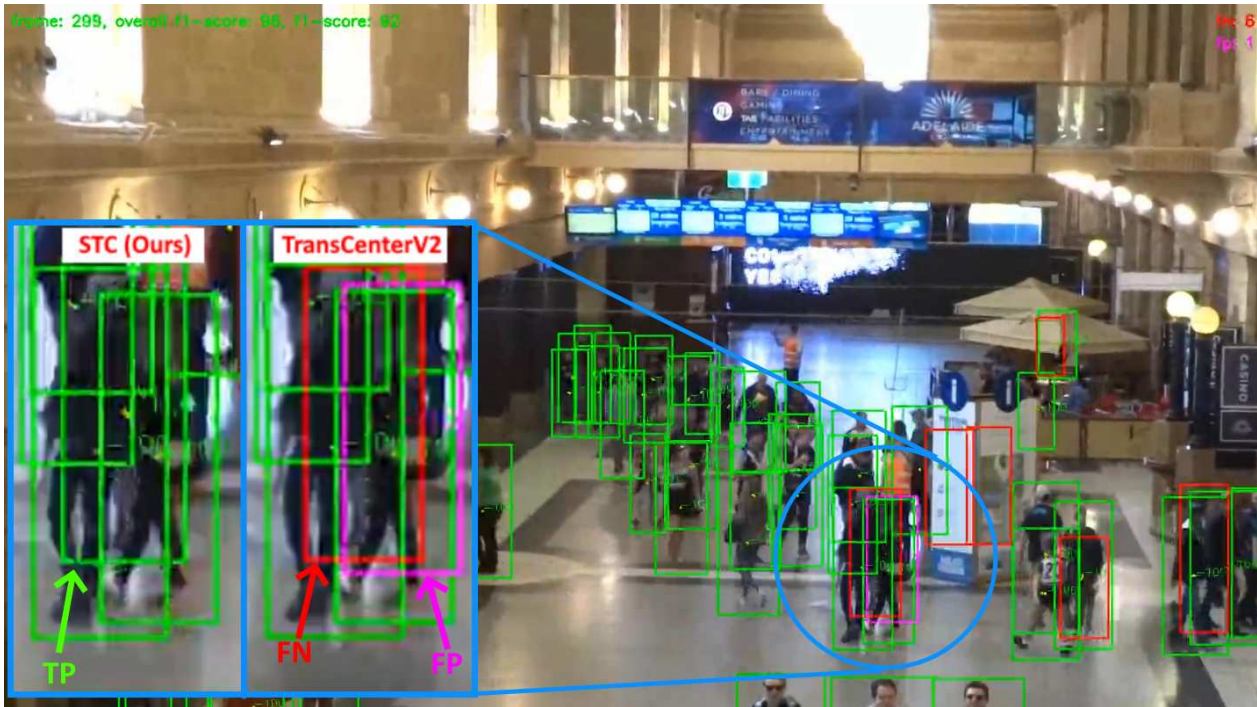


Figure 6: Visualization of a specific scenario in the results of a tracker based only on transformer (TransCenterV2 [19]). The full frame shows the results of the TransCenterV2 tracker compared to the ground truth: green boxes are True Positive (TP), red boxes are False negative (FN) and pink boxes are False Positive (FP). The zoom-in image shows the area of the error in the frame with the original TransCenter on the right and with our STC tracker on the left. The results are from the MOT20-01 video on frame 299.

- [21] K. He, X. Zhang, S. Ren, and J. Sun, “Deep residual learning for image recognition,” in *2016 IEEE/CVF Conference on Computer Vision and Pattern Recognition (CVPR)*, L. Agapito, T. Berg, J. Kosecka, and L. Zelnik-Manor, Eds., IEEE, Jun. 2016, pp. 770–778, ISBN: 978-1-4673-8851-1. DOI: [10.1109/CVPR.2016.90](https://doi.org/10.1109/CVPR.2016.90).
- [22] W. Wang, E. Xie, X. Li, *et al.*, “Pvt v2: Improved baselines with pyramid vision transformer,” *Computational Visual Media*, vol. 8, pp. 415–424, 3 Sep. 2022, ISSN: 2096-0433. DOI: [10.1007/s41095-022-0274-8](https://doi.org/10.1007/s41095-022-0274-8).
- [23] N. Carion, F. Massa, G. Synnaeve, N. Usunier, A. Kirillov, and S. Zagoruyko, “End-to-end object detection with transformers,” *arXiv*, May 2020.
- [24] Y. Zhang, C. Wang, X. Wang, W. Zeng, and W. Liu, “Fairmot: On the fairness of detection and re-identification in multiple object tracking,” *IJCV*, vol. 129, pp. 3069–3087, 11 Nov. 2021. DOI: [10.1007/s11263-021-01513-4](https://doi.org/10.1007/s11263-021-01513-4).
- [25] Y. Du, Y. Song, B. Yang, and Y. Zhao, “Strongsort: Make deepsort great again,” *arXiv*, Feb. 2022.
- [26] H. Rezatofighi, N. Tsoi, J. Gwak, A. Sadehian, I. Reid, and S. Savarese, “Generalized intersection over union: A metric and a loss for bounding box regression,” in *2019 IEEE/CVF Conference on Computer Vision and Pattern Recognition (CVPR)*, A. Gupta, D. Hoiem, G. Hua, and Z. Tu, Eds., IEEE, Jun. 2019, pp. 658–666, ISBN: 978-1-7281-3293-8. DOI: [10.1109/CVPR.2019.00075](https://doi.org/10.1109/CVPR.2019.00075).
- [27] H. Wang, M. Yao, G. Jiang, Z. Mi, and X. Fu, “Graph-collaborated auto-encoder hashing for multi-view binary clustering,” *IEEE Transactions on Neural Networks and Learning Systems*, pp. 1–13, 2023. DOI: [10.1109/TNNLS.2023.3239033](https://doi.org/10.1109/TNNLS.2023.3239033).
- [28] H. Wang, J. Peng, D. Chen, G. Jiang, T. Zhao, and X. Fu, “Attribute-guided feature learning network for vehicle reidentification,” *IEEE MultiMedia*, vol. 27, no. 4, pp. 112–121, 2020. DOI: [10.1109/MMUL.2020.2999464](https://doi.org/10.1109/MMUL.2020.2999464).
- [29] H. Wang, Y. Wang, Z. Zhang, *et al.*, “Kernelized multiview subspace analysis by self-weighted learning,” *IEEE Transactions on Multimedia*, vol. 23,

- pp. 3828–3840, 2021. DOI: [10 . 1109 / TMM . 2020 . 3032023](https://doi.org/10.1109/TMM.2020.3032023).
- [30] H. Wang, G. Jiang, J. Peng, R. Deng, and X. Fu, “Towards adaptive consensus graph: Multi-view clustering via graph collaboration,” *IEEE Transactions on Multimedia*, pp. 1–13, 2022. DOI: [10 . 1109 / TMM . 2022 . 3212270](https://doi.org/10.1109/TMM.2022.3212270).
- [31] M. Ye, J. Shen, G. Lin, T. Xiang, L. Shao, and S. C. H. Hoi, “Deep learning for person re-identification: A survey and outlook,” *IEEE Transactions on Pattern Analysis and Machine Intelligence*, vol. 44, no. 6, pp. 2872–2893, 2022. DOI: [10 . 1109 / TPAMI . 2021 . 3054775](https://doi.org/10.1109/TPAMI.2021.3054775).
- [32] L. Zheng, M. Tang, Y. Chen, G. Zhu, J. Wang, and H. Lu, “Improving multiple object tracking with single object tracking,” in *2021 IEEE/CVF Conference on Computer Vision and Pattern Recognition (CVPR)*, D. Forsyth, G. Gkioxari, T. Tuytelaars, R. Yang, and J. Yu, Eds., IEEE, Jun. 2021, pp. 2453–2462, ISBN: 978-1-6654-4509-2. DOI: [10 . 1109 / CVPR46437 . 2021 . 00248](https://doi.org/10.1109/CVPR46437.2021.00248).
- [33] E. Yu, Z. Li, S. Han, and H. Wang, “Relationtrack: Relation-aware multiple object tracking with decoupled representation,” *IEEE Transactions on Multimedia*, pp. 1–1, 2022, ISSN: 1520-9210. DOI: [10 . 1109 / TMM . 2022 . 3150169](https://doi.org/10.1109/TMM.2022.3150169).
- [34] C. Liang, Z. Zhang, X. Zhou, B. Li, S. Zhu, and W. Hu, “Rethinking the competition between detection and reid in multiobject tracking,” *IEEE Transactions on Image Processing*, vol. 31, pp. 3182–3196, 2022, ISSN: 1057-7149. DOI: [10 . 1109 / TIP . 2022 . 3165376](https://doi.org/10.1109/TIP.2022.3165376).
- [35] Q. Wang, Y. Zheng, P. Pan, and Y. Xu, “Multiple object tracking with correlation learning,” in *2021 IEEE/CVF Conference on Computer Vision and Pattern Recognition (CVPR)*, D. Forsyth, G. Gkioxari, T. Tuytelaars, R. Yang, and J. Yu, Eds., IEEE, Jun. 2021, pp. 3875–3885, ISBN: 978-1-6654-4509-2. DOI: [10 . 1109 / CVPR46437 . 2021 . 00387](https://doi.org/10.1109/CVPR46437.2021.00387).
- [36] S. Kim, J. Lee, and B. C. Ko, “SSL-MOT: Self-supervised learning based multi-object tracking,” *Applied Intelligence*, vol. 53, no. 1, pp. 930–940, Apr. 2022. DOI: [10 . 1007 / s10489 - 022 - 03473 - 9](https://doi.org/10.1007/s10489-022-03473-9). [Online]. Available: <https://doi.org/10.1007/s10489-022-03473-9>.
- [37] H. Luo, Y. Gu, X. Liao, S. Lai, and W. Jiang, “Bag of tricks and a strong baseline for deep person re-identification,” I. S. Kweon, N. Paragios, M.-H. Yang, and S. Lazebnik, Eds., IEEE, Mar. 2019.
- [38] L. He, X. Liao, W. Liu, X. Liu, P. Cheng, and T. Mei, “Fastreid: A pytorch toolbox for general instance re-identification,” *arXiv*, Jun. 2020.
- [39] H. Zhang, C. Wu, Z. Zhang, *et al.*, “Resnest: Split-attention networks,” *CVPR*, Apr. 2020.
- [40] P. Dendorfer, H. Rezatofighi, A. Milan, *et al.*, “Mot20: A benchmark for multi object tracking in crowded scenes,” *arXiv*, Mar. 2020.
- [41] K. Bernardin and R. Stiefelhagen, “Evaluating multiple object tracking performance: The clear mot metrics,” *EURASIP Journal on Image and Video Processing*, vol. 2008, pp. 1–10, 2008, ISSN: 1687-5176. DOI: [10 . 1155 / 2008 / 246309](https://doi.org/10.1155/2008/246309).
- [42] Francesco, Z. Roger, C. Rita, T. C. R. Ergys, and Solera, “Performance measures and a data set for multi-target, multi-camera tracking,” H. H. Gang and Jégou, Eds., Springer International Publishing, 2016, pp. 17–35, ISBN: 978-3-319-48881-3.
- [43] J. Luiten, A. Osep, P. Dendorfer, *et al.*, “Hota: A higher order metric for evaluating multi-object tracking,” *arXiv*, Sep. 2020. DOI: [10 . 1007 / s11263 - 020 - 01375 - 2](https://doi.org/10.1007/s11263-020-01375-2).
- [44] Y. Wang, K. Kitani, and X. Weng, “Joint object detection and multi-object tracking with graph neural networks,” in *2021 IEEE International Conference on Robotics and Automation (ICRA)*, IEEE, Ed., IEEE, May 2021, pp. 13 708–13 715, ISBN: 978-1-7281-9077-8. DOI: [10 . 1109 / ICRA48506 . 2021 . 9561110](https://doi.org/10.1109/ICRA48506.2021.9561110).
- [45] Y. Zhang, H. Sheng, Y. Wu, S. Wang, W. Ke, and Z. Xiong, “Multiplex labeling graph for near-online tracking in crowded scenes,” *IEEE Internet of Things Journal*, vol. 7, pp. 7892–7902, 9 Sep. 2020, ISSN: 2327-4662. DOI: [10 . 1109 / JIOT . 2020 . 2996609](https://doi.org/10.1109/JIOT.2020.2996609).
- [46] C. Shan, C. Wei, B. Deng, *et al.*, “Tracklets predicting based adaptive graph tracking,” *arXiv*, Oct. 2020.
- [47] L. Chen, H. Ai, Z. Zhuang, and C. Shang, “Real-time multiple people tracking with deeply learned candidate selection and person re-identification,” in *2018 IEEE International Conference on Multimedia and Expo (ICME)*, IEEE, Ed., IEEE, Jul. 2018, pp. 1–6, ISBN: 978-1-5386-1737-3. DOI: [10 . 1109 / ICME . 2018 . 8486597](https://doi.org/10.1109/ICME.2018.8486597).
- [48] J. He, Z. Huang, N. Wang, and Z. Zhang, “Learnable graph matching: Incorporating graph partitioning with deep feature learning for multiple object tracking,” in *2021 IEEE/CVF Conference on Computer Vision and Pattern Recognition (CVPR)*, D. Forsyth, G. Gkioxari, T. Tuytelaars, R. Yang, and J. Yu, Eds., Mar. 2021, pp. 5299–5309.

- [49] B. Shuai, A. Berneshawi, X. Li, D. Modolo, and J. Tighe, “Siammot: Siamese multi-object tracking,” in *2021 IEEE/CVF Conference on Computer Vision and Pattern Recognition (CVPR)*, D. Forsyth, G. Gkioxari, T. Tuytelaars, R. Yang, and J. Yu, Eds., IEEE, Jun. 2021, pp. 12 367–12 377, ISBN: 978-1-6654-4509-2. DOI: [10 . 1109 / CVPR46437 . 2021.01219](https://doi.org/10.1109/CVPR46437.2021.01219).
- [50] X. Zhou, V. Koltun, and P. Krähenbühl, “Tracking objects as points,” in *Computer Vision – ECCV 2020*, A. Vedaldi, H. Bischof, T. Brox, and J.-M. Frahm, Eds., Cham: Springer International Publishing, 2020, pp. 474–490, ISBN: 978-3-030-58548-8.
- [51] J. Wu, J. Cao, L. Song, Y. Wang, M. Yang, and J. Yuan, “Track to detect and segment: An online multi-object tracker,” in *2021 IEEE/CVF Conference on Computer Vision and Pattern Recognition (CVPR)*, D. Forsyth, G. Gkioxari, T. Tuytelaars, R. Yang, and J. Yu, Eds., IEEE, Jun. 2021, pp. 12 347–12 356, ISBN: 978-1-6654-4509-2. DOI: [10 . 1109 / CVPR46437 . 2021.01217](https://doi.org/10.1109/CVPR46437.2021.01217).
- [52] P. Tokmakov, J. Li, W. Burgard, and A. Gaidon, “Learning to track with object permanence,” D. Damen, T. Hassner, C. Pal, and Y. Sato, Eds., IEEE, Oct. 2021, pp. 10 840–10 849, ISBN: 978-1-6654-2812-5. DOI: [10 . 1109 / ICCV48922 . 2021 . 01068](https://doi.org/10.1109/ICCV48922.2021.01068).
- [53] F. Yang, X. Chang, S. Sakti, Y. Wu, and S. Nakamura, “Remot: A model-agnostic refinement for multiple object tracking,” *Image and Vision Computing*, vol. 106, p. 104 091, Feb. 2021, ISSN: 02628856. DOI: [10.1016/j.imavis.2020.104091](https://doi.org/10.1016/j.imavis.2020.104091).
- [54] Z. Qin and C. R. Shelton, “Improving multi-target tracking via social grouping,” in *2012 IEEE/CVF Conference on Computer Vision and Pattern Recognition (CVPR)*, IEEE, Ed., IEEE, Jun. 2012, pp. 1972–1978, ISBN: 978-1-4673-1228-8. DOI: [10 . 1109 / CVPR . 2012 . 6247899](https://doi.org/10.1109/CVPR.2012.6247899).
- [55] D. Forsyth, G. Gkioxari, T. Tuytelaars, R. Yang, and J. Yu, Eds., 2021.
- [56] I. S. Kweon, N. Paragios, M.-H. Yang, and S. Lazebnik, Eds., *2019 IEEE/CVF International Conference on Computer Vision (ICCV)*, IEEE, 2019.